J|A|C|S
ARTICLES

Published on Web 10/06/2009

Ferromagnetic $CoPt_3$ Nanowires: Structural Evolution from fcc to Ordered $L1_2$

Hao Ming Chen,[†] Chia Fen Hsin,[†] Po Yuan Chen,[‡] Ru-Shi Liu,*[,†] Shu-Fen Hu,[§] Chao-Yuan Huang,[‡] Jyh-Fu Lee,[||] and Ling-Yun Jang[||]

Department of Chemistry, National Taiwan University, Taipei 106, Taiwan, Institute of Electro-optical Science and Technology, National Taiwan Normal University, Taipei 116, Taiwan, Department of Physics, National Taiwan Normal University, Taipei 116, Taiwan, and National Synchrotron Radiation Research Center, Hsinchu 300, Taiwan

Received July 22, 2009; E-mail: rsliu@ntu.edu.tw

Abstract: This investigation demonstrates the magnetic properties and nanostructures of $CoPt_3$ wire arrays that were fabricated by electrodeposition using a porous alumina template. The X-ray absorption analysis clearly verified the occurrence of a phase transition in $CoPt_3$ nanowires. This phase transition significantly influences the magnetic properties and enhances coercivity and squareness. The phase transition of $CoPt_3$ nanowires was from a random alloy distribution to anisotropically ordered $CoPt_3$ ($L1_2$). The thermally induced phase transition of $CoPt_3$ nanowires to ordered $L1_2$ $CoPt_3$ through a "cluster-in-cluster" intermediate state *via* interdiffusion processes is revealed. The mechanism exhibited by these $CoPt_3$ nanowires is proposed to explain the strong correlation between their magnetic character and their atomic distribution.

Introduction

The synthesis of nanostructural materials has been an important area of research for decades owing to their extensive use in electronics, photonics, catalysis, information storage, optical sensing, biological labeling, imaging, and surface-enhanced Raman scattering studies.[1−5] In particular, the fabrication of metal nanowires has recently attracted substantial attention because they have unique magnetic properties and other potential technological applications.[6] One effective method of fabricating metal nanowires is electrodeposition, in which metals and alloys are electrochemically deposited into a porous template. The most commonly used templates are porous anodic oxide films that are produced from aluminum plates; they have been used to form products which various morphologies.[7] The anodic oxidized alumina films have the advantages over others of chemical stability and easy control of nanopores.[8] Aluminum anodizing technology has been developed to such a degree that the dimensions and distribution of pores in the film can be artificially controlled by preindentation.[9] Significant progress in the preparation of transition metal nanowires has been achieved by utilizing porous alumina templates. Such schemes have been developed for iron, cobalt, nickel, and alloy nanowires.[10,11] Nanowires of magnetic materials (Fe, Co, Ni, FePt, CoPt, and others) attract special attention because of their potential in ultrahigh-density magnetic data storage devices. Co−Pt alloy films exhibit strong perpendicular magnetic anisotropy and high chemical stability.[12]

[†] National Taiwan University.
[‡] Institute of Electro-optical Science and Technology, National Taiwan Normal University.
[§] Department of Physics, National Taiwan Normal University.
[||] National Synchrotron Radiation Research Center.

(1) Electronics and photonics: (a) El-Sayed, M. A. *Acc. Chem. Res.* **2001**, *34*, 257. (b) Chen, S.; Yang, Y. *J. Am. Chem. Soc.* **2002**, *124*, 5280.
(2) Catalysis: (a) Lewis, L. N. *Chem. Rev.* **1993**, *93*, 2693. (b) Chen, M. S.; Goodman, D. W *Science* **2004**, *306*, 252. (c) Valden, M.; Lai, X.; Goodman, D. W. *Science* **1998**, *281*, 1647. (d) Sinha, A. K.; Seelan, S.; Tsubota, S.; Haruta, M. *Angew. Chem., Int. Ed.* **2004**, *43*, 1546. (e) Zhou, S.; Mcllwrath, K.; Jackson, G.; Eichhorn, B. *J. Am. Chem. Soc.* **2006**, *128*, 1780.
(3) Information storage: (a) Peyser, L. A.; Vinson, A. E.; Bartko, A. P.; Dickson, R. M. *Science* **2001**, *291*, 103. (b) Chen, H. M.; Liu, R.-S.; Li, H.; Zeng, H. C. *Angew. Chem., Int. Ed.* **2006**, *45*, 2713. (c) Kang, S.; Harrell, J. W.; Nikles, D. E. *Nano Lett.* **2002**, *2*, 1033.
(4) Optical sensing, biological labeling, and imaging: (a) Storhoff, J. J.; Elghanian, R.; Mucic, R. C.; Mirkin, C. A.; Letsinger, R. L. *J. Am. Chem. Soc.* **1998**, *120*, 1959. (b) Park, S.-J.; Taton, T. A.; Mirkin, C. A. *Science* **2002**, *295*, 1503. (c) Charles Cao, Y. W.; Jin, R.; Mirkin, C. A. *Science* **2002**, *297*, 1536. (d) Rosi, N. L.; Giljohann, D. A.; Thaxton, C. S.; Lytton-Jean, A. K. R.; Han, M. S.; Mirkin, C. A. *Science* **2006**, *312*, 1027. (e) Chen, H. M.; Peng, H.-C.; Liu, R.-S.; Asakura, K.; Lee, C.-L.; Lee, J.-F.; Hu, S.-F. *J. Phys. Chem. B* **2005**, *109*, 19553. (f) Kamat, P. V. *J. Phys. Chem. B* **2002**, *106*, 7729.
(5) SERS: (a) Nie, S.; Emory, S. R. *Science* **1997**, *275*, 1102. (b) Tessier, P. M.; Velev, O. D.; Kalambur, A. T.; Rabolt, J. F.; Lenhoff, A. M.; Kaler, E. W. *J. Am. Chem. Soc.* **2000**, *122*, 9554. (c) Xiong, Y.; McLellan, J. M.; Chen, J.; Yin, Y.; Li, Z.-Y.; Xia, Y. *J. Am. Chem. Soc.* **2005**, *127*, 17118.
(6) Kline, T. R.; Tian, M.; Wand, J.; Sen, A.; Chan, M. W. H.; Mallouk, T. E. *Inorg. Chem.* **2006**, *45*, 7555.
(7) (a) Whitney, T. M.; Jiang, J. S.; Searson, P. C.; Chien, C. L. *Science* **1993**, *261*, 1316. (b) Sander, M. S.; Gao, H. *J. Am. Chem. Soc.* **2005**, *127*, 12158. (c) Nicewarner-Pena, S. R.; Freeman, R. G.; Reiss, B. D.; He, L.; Pena, D. J.; Walton, I. D.; Cromer, R.; Keating, C. D.; Natan, M. J. *Science* **2001**, *294*, 137. (d) Luo, J.; Zhang, L.; Zhang, Y.; Zhu, J. *Adv. Mater.* **2002**, *14*, 1413. (e) Lahav, M.; Weiss, E. A.; Xu, Q.; Whitesides, G. M. *Nano Lett.* **2006**, *6*, 2166. (f) Xue, F. H.; Fei, G. T.; Wu, B.; Cui, P.; Zhang, L. D. *J. Am. Chem. Soc.* **2005**, *127*, 15348.
(8) (a) Martin, C. R. *Science* **1994**, *266*, 1961. (b) Masuda, H.; Fukuda, K. *Science* **1995**, *268*, 1466.
(9) (a) Masuda, H.; Hasegwa, F. *J. Electrochem. Soc.* **1997**, *144*, L127. (b) Zhao, S.; Roberge, H.; Yelon, A.; Veres, T. *J. Am. Chem. Soc.* **2006**, *128*, 12352. (c) Jessensky, O.; Muller, F.; Gosele, U. *Appl. Phys. Lett.* **1998**, *72*, 1173. (d) Li, A. P.; Muller, F.; Birner, A.; Nielsch, A.; Gosele, U. *J. Appl. Phys.* **1998**, *84*, 6023. (e) Xiong, G.; Elam, J. W.; Feng, H.; Han, C. Y.; Wang, H.-H.; Iton, L. E.; Curtiss, L. A.; Pellin, M. J.; Kung, M.; Kung, H.; Stair, P. C. *J. Phys. Chem. B* **2005**, *109*, 14059.

10.1021/ja906103p CCC: $40.75

In this investigation, the magnetic nanomaterial $CoPt_3$ is used as a model system to understand the alloying process that is critical in systems that exhibit such magnetic properties as high magnetic anisotropy and magneto-optic Kerr effects.[13] Comprehensive structural characterizations of bimetallic nanomaterials and their phase transformation processes are crucial. Although transmission electron microscopy (TEM) has been a powerful tool for probing nanomaterials, it is limited in the amount of information it can provide on the chemical bonding and structural characterization of complex multicomponent materials such as nanoalloys. In contrast, X-ray absorption spectroscopy (XAS) can provide valuable structural and chemical information about nanostructures. The study of the extended X-ray absorption fine structure (EXAFS) has been particularly effective in providing structural information about noncrystalline and crystalline materials.[14] EXAFS is a short-range probe of structure and yield results concerning local correlations around the absorbing atom, specifically the nearest-neighbor interatomic distances and coordination numbers. The use of monochromatic radiation makes EXAFS element-selective and consequently well suited to samples that contain more than one type of metal atom, or substrate lattices, which interfere with diffraction measurement. While extensive XAS studies of noble metals and their alloys have been conducted, few have been performed on magnetic nanomaterials. This study demonstrates the formation of bimetallic nanowires and monitors their ferromagnetic phase transitions from solid solution alloy to the chemical ordering phase (with an $L1_2$ structure and an fcc lattice) using XAS.

Experimental Section

Chemicals and Materials. Hydrogen hexachloroplatinate(IV) hydrate, cobalt(II) sulfate heptahydrate (99%), mercury(II) chloride (99.5%), sodium hydroxide (96%), phosphoric acid (85%), and oxalic acid (99%) were obtained from Acros Organics and used without further purification. Potassium dichromate from YAKURI was used as received. The water used throughout this investigation was of reagent grade and was produced using a Milli-Q SP ultrapure-water purification system from Nihon Millipore Ltd., Tokyo.

Fabrication Method of Porous Alumina Templates. The starting materials were highly pure (99.99%) aluminum foils. Al foils were anodized at 40 V in 5 wt % oxalic acid for 3 h at 5 °C. The anodic alumina films were dissolved in a mixed solution of 1.8 wt % H_2CrO_4 and 6 wt % H_3PO_4 at 60 °C for 1 h. These textured Al specimens were anodized again for 23 h under the same conditions as were applied in the initial anodizing step. The Al substrates were removed in saturated $HgCl_2$ solution, and the barrier layer was then removed using 5 wt % H_3PO_4 solutions at room temperature. An approximately 500 nm thick layer of gold thermal evaporated on one side of an alumina template served as the working electrode, and the deposition rate was 10 Å/s.

Fabrication of CoPt Nanowires. The electrolyte used to electrodeposit CoPt nanowires had the following composition: H_2PtCl_6 (0.002 M), $CoSO_4$ (0.1 M), and H_3BO_3 (0.5 M). Deposition was performed in a three-electrode cell using a platinum counter electrode and a Ag/AgCl reference electrode at room temperature. Then, a direct constant potential of 0.73 V was used to deposit CoPt nanowires. Following electrodeposition, the CoPt nanowire arrays were annealed for 5 h at various temperatures in 5% H_2/N_2. The AAO template was removed by dissolving it in a 1 M NaOH aqueous solution for 30 min. It was then washed numerous times with distilled water and ethanol.

Characterization of Nanowires. The chemical composition of the nanowires was determined by both inductively coupled plasma atomic emission spectroscopy (ICP-AES), performed using a Perkin-Elmer Plasma 40 spectrometer, and energy-dispersive X-ray analysis (EDS), performed using a JEOL JSM-6700F field emission scanning electron microscope (FE-SEM) that was equipped with an EDS probe. The crystallographic structures of the CoPt nanowires arrays were analyzed by X-ray powder diffraction (XRD) using an X'Pert PRO diffractometer using Cu Kα radiation ($\lambda = 1.5418$ Å). Magnetic studies were carried out using a commercial vibrating sample magnetometer (VSM) with fields of up to 12 T at room temperature. Measurements were made on a silica microslide perpendicular and parallel to the magnetic field. A series of EXAFS measurements of the synthesized samples were made using synchrotron radiation at room temperature. Measurements were made at the Pt L_3-edge (11564 eV) and the Co K-edge (7709 eV) with the sample held at room temperature.

EXAFS Data Analysis. The backscattering amplitude and phase shift functions for specific atom pairs were calculated *ab initio* using the FEFF7 code. X-ray absorption data were analyzed using standard procedures, including pre-edge and postedge background subtraction, normalization with respect to edge height, Fourier transformation, and nonlinear least-squares curve fitting.[15] The normalized k^3-weighted EXAFS spectra, $k^3x(k)$, were Fourier-transformed in a k range from 3 to 14 $Å^{-1}$, to evaluate the contribution of each bond pair to the Fourier transform (FT) peak. The experimental Fourier-filtered spectra were obtained by performing an inverse Fourier transformation with a Hanning window function with r between 1.8 and 3.2 Å. The S_0^2 (amplitude reduction factor) values of the Co and Pt atoms were fixed at 0.85 and 0.83, to determine the structural parameters of each bond pair. Co and Pt edge data were analyzed simultaneously. The Debye−Waller factors, interatomic distance, and coordination numbers of Co−Pt and Pt−Co bonds were constrained to be the same in both analyses of Co K- and Pt L_3-edges. The Wiggler-C beamline of the National Synchrotron Radiation Research Center (NSRRC), Taiwan, was designed for such experiments.

(10) (a) Chu, S.-Z.; Wada, K.; Inoue, S.; Todoroki, S.-I.; Takahashi, Y. K.; Hono, K. *Chem. Mater.* **2002**, *14*, 4595. (b) Tian, F.; Zhu, J.; Wei, D.; Shen, Y. T. *J. Phys. Chem. B* **2005**, *109*, 14852. (c) Pan, H.; Liu, B.; Yi, J.; Poh, C.; Lim, S.; Ding, J.; Feng, Y.; Huan, C. H. A.; Lin, J. *J. Phys. Chem. B* **2005**, *109*, 3094. (d) Qin, J.; Nogues, J.; Mikhaylova, M.; Roig, A.; Munoz, J. S.; Muhammed, M. *Chem. Mater.* **2005**, *17*, 1829.

(11) (a) Guo, Y.-G.; Wan, L.-J.; Zhu, C.-F.; Yang, D.-L.; Chen, D.-M.; Bai, C.-L. *Chem. Mater.* **2003**, *15*, 664. (b) Ji, G.; Cao, J.; Zhang, F.; Xu, G.; Su, H.; Tang, S.; Gu, B.; Du, Y. *J. Phys. Chem. B* **2005**, *109*, 17100. (c) Chu, S.-Z.; Inoue, S.; Wada, K.; Kurashima, K. *J. Phys. Chem. B* **2004**, *108*, 5582. (d) Choi, J.-r.; Oh, S. J.; Ju, H.; Cheon, J. *Nano Lett.* **2005**, *5*, 2179. (e) Liu, F.; Lee, J. Y.; Zhou, W. *J. Phys. Chem. B* **2004**, *108*, 17959. (f) Ji, G. B.; Tang, S. L.; Gu, B. X.; Du, Y. W. *J. Phys. Chem. B* **2004**, *108*, 8862.

(12) (a) Shapiro, A. L.; Rooney, P. W.; Tran, M. Q.; Hellman, F.; Ring, K. M.; Kavanagh, K. L.; Rellinghaus, B.; Weller, D. *Phys. Rev. B* **1999**, *60*, 12826. (b) Lin, C.-J.; Gorman, G. L. *Appl. Phys. Lett.* **1992**, *61*, 2726. (c) Chang, G.; Lee, Y.; Rhee, J.; Lee, J.; Jeong, K.; Whang, C. *Phys. Rev. Lett.* **2001**, *87*, 067208-1. (d) Tyson, T. A.; Conradson, S. D.; Farrow, R. F. C.; Jones, B. A. *Phys. Rev. B* **1996**, *54*, R3702.

(13) (a) Ely, T. O.; Pan, C.; Amiens, C.; Chaudret, B.; Dassenoy, F.; Lecante, P.; Casanove, M.-J.; Mosset, A.; Respaud, M.; Broto, J.-M. *J. Phys. Chem. B* **2000**, *104*, 695. (b) Harp, G. R.; Weller, D.; Rabedeau, T. A.; Farrow, R. F. C.; Toney, M. F. *Phys. Rev. Lett.* **1993**, *71*, 2493. (c) Mehaddene, T.; Kentzinger, E.; Hennion, B.; Tanaka, K.; Numakura, H.; Marty, A.; Parasote, V.; Cadeville, M. C.; Zemirli, M.; Pierron-Bohnes, V. *Phys. Rev. B* **2004**, *69*, 024304.

(14) (a) Penner-Hahn, J. E. *Coord. Chem. Rev.* **1999**, *190*, 1101. (b) Chen, H. M.; Liu, R.-S.; Asakura, K.; Jang, L.-Y.; Lee, J.-F. *J. Phys. Chem. C* **2007**, *111*, 18550. (c) Lee, W.-R.; Kim, M. G.; Choi, J.-R.; Park, J.-I.; Ko, S. J.; Oh, S. J.; Cheon, J. *J. Am. Chem. Soc.* **2005**, *127*, 16090. (d) Polarz, S.; Neues, F.; van den Berg, M. W. E.; Grunert, W.; Khodeir, L. *J. Am. Chem. Soc.* **2005**, *127*, 12028. (e) Jensen, M. P.; Dzielawa, J. A.; Rickert, P.; Dietz, M. L *J. Am. Chem. Soc.* **2002**, *124*, 10664. (f) Chen, H. M.; Hsin, C. F.; Liu, R. S.; Lee, J.-F.; Jang, L.-Y. *J. Phys. Chem. C* **2007**, *111*, 5909.

(15) Iwasawa, Y. *X-ray Absorption Fine Structure for Catalysts and Surfaces*; World Scientific: Singapore, 1996.

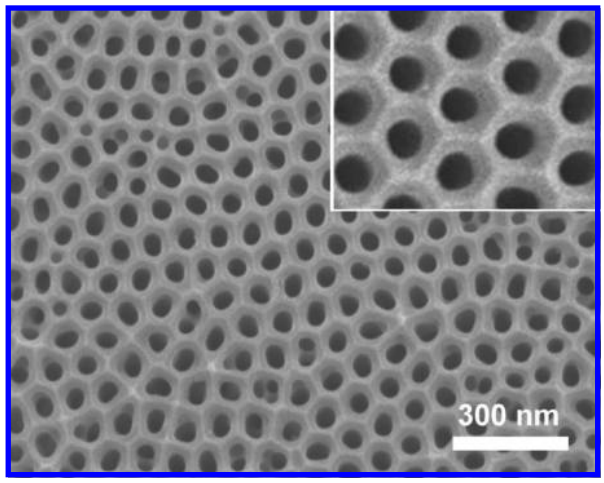

Figure 1. FE-SEM top-view micrographs of anodic alumina oxide templates.

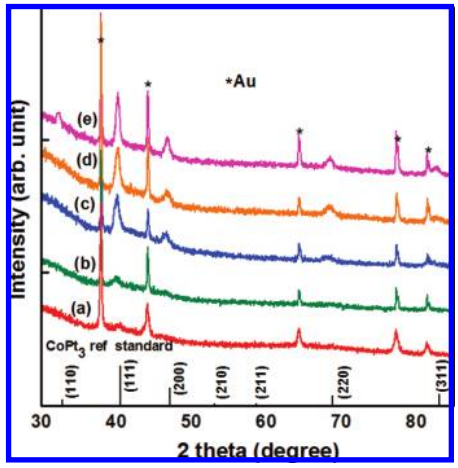

Figure 2. XRD patterns of $Co_{26}Pt_{74}$ nanowires: (a) as-prepared and annealed under flowing N_2/H_2 (95/5) for 5 h at temperatures of (b) 400, (c) 500, (d) 600, (e) 700 °C and standard $CoPt_3$ $L1_2$ (JCPDS file no. 29-0499).

Results and Discussion

Morphological Analysis of Template. Figure 1 presents the top-view FE-SEM micrographs of the anodic alumina oxide (AAO) templates after chemical etching using phosphoric acid solution. The hexagonal close-packed arrays in Figure 1 have identical pore diameters of approximately 60 nm with a standard deviation of 5 nm; the pore density is $\sim 10^{10}$ pores/cm^2. The diameter and the gaps among the pores are based on the applied voltage.[8] The applied voltage can be adjusted, and various electrolytes are used to prepare AAO templates with various diameters and lengths.

Structural Analysis via XRD. Changes in the crystalline structure of nanowires upon annealing were examined by X-ray diffraction. Figure 2 displays a series of XRD patterns for $Co_{26}Pt_{74}$ (composition was determined by ICP-AES) nanowires for various annealing temperatures and a constant annealing time of 5 h. The conductive Au back electrode was responsible for the presence of an fcc gold structure. As-prepared (Figure 2a) nanowires had a weakly chemical disordered fcc structure. Figure 2c exhibits a higher-intensity (111) diffraction peak than was obtained by annealing at 400 °C (Figure 2b), suggesting that annealing treatment leads to the growth of the CoPt nanocrystal. At an annealing temperature of 600 °C, the XRD patterns reveal only an fcc phase. Careful examination of the diffraction pattern e in Figure 2 demonstrates that (110) reflection associated with the chemically ordered $L1_2$ phase of $CoPt_3$ appeared after 700 °C of heat treatment. Accordingly, following annealing at a temperature of below 700 °C, only the phase with the fcc structure was observed. Consequently, annealing rearranges the Co and Pt atoms into a long-range chemically ordered $L1_2$ structure, as revealed by the presence of (110) reflections from the sample that had been annealed at 700 °C. Notably, the ratio between the intensities of the (110) and (111) diffraction peaks (0.06 versus 1) is slightly less than the conventional value for the $L1_2$ $CoPt_3$ phase (0.1 versus 1). This observation confirms that nanowires partially transformed from the disordered fcc structure to the ordered $L1_2$.

Morphological Analysis of CoPt Nanowires. Figure 3a presents a typical FE-SEM image of as-prepared CoPt nanowires. The length of as-prepared nanowires is ~ 10 μm, which can be controlled by varying electrochemical deposition time. The EDS spectrum of the nanowires establishes the presence of only cobalt, platinum, aluminum, and oxygen (see Supporting Information S1). The results of ICP-AES and EDS composition analyses were in good agreement and revealed that the nanowires comprised Co and Pt. These results clearly indicate that an ordered CoPt nanowire array was deposited inside the channels of the alumina membrane. The mean chemical composition (atom %) of the nanowires, determined by EDS microanalysis, was $Co_{26}Pt_{74}$, whose stoichiometry is close to the expected 1:3 stoichiometry. The composition was controlled most effectively by optimizing the experimental procedure that yielded the $Co_{26}Pt_{74}$ stable phase. Figure 3b shows a magnified FE-SEM image of the as-prepared $CoPt_3$ nanowires that were obtained by this electrochemical method in an AAO template with a diameter of approximately 60 nm. The nanowires are continuous and arranged roughly parallel to one another, and all have a uniform diameter of $\sim$50 nm, which is slightly less than the diameter of the pores in the template. This result is well explained by the shrinkage that is caused by the densification and the removal of water.[16] Most specifically, some broken nanowires after the AAO template was removed have been observed. This may be explained by the rapid electrochemical deposition and lattice mismatch (Co lattice constant $a = 3.544$ Å, JCPDS file no. 89-4307; Pt lattice constant $a = 3.920$ Å, JCPDS file no. 87-0646). A fast growth rate and the availability of plenty of metal ions resulted in crystal growth much less selective in direction and hence produced a great amount of structural defects. Figure 3c and 3d show FESEM images of $CoPt_3$ nanowires after annealing (700 °C, 5 h) in a 5% H_2/N_2 atmosphere. The $CoPt_3$ nanowires are of almost equal diameter (nearly 50 nm), and the surface is smoother than that of as-prepared nanowires, the average length being ~ 13 μm. The $CoPt_3$ nanowires are laterally constrained by the surrounding alumina templates, and the nanowires diameter and morphology are maintained without coarsening during the thermal treatment. The segmented $CoPt_3$ nanowires (Figure 3b) became smooth and continuous, which indicates that thermal treatment led to the migration of atoms and the rearrangement of the lattice structure, consistent with the XRD observations. As a result, annealing at high temperature increased structural chemical ordering. Therefore, as mentioned above, complete fcc-to-$L1_2$ transformation was achieved at 700 °C, 20 °C lower than the temperature for pure $CoPt_3$ phase transformation.[13c] In the solid

(16) Miao, Z.; Xu, D.; Ouyang, J.; Guo, G.; Zhao, X.; Tang, Y. *Nano Lett.* **2002**, *2*, 717.

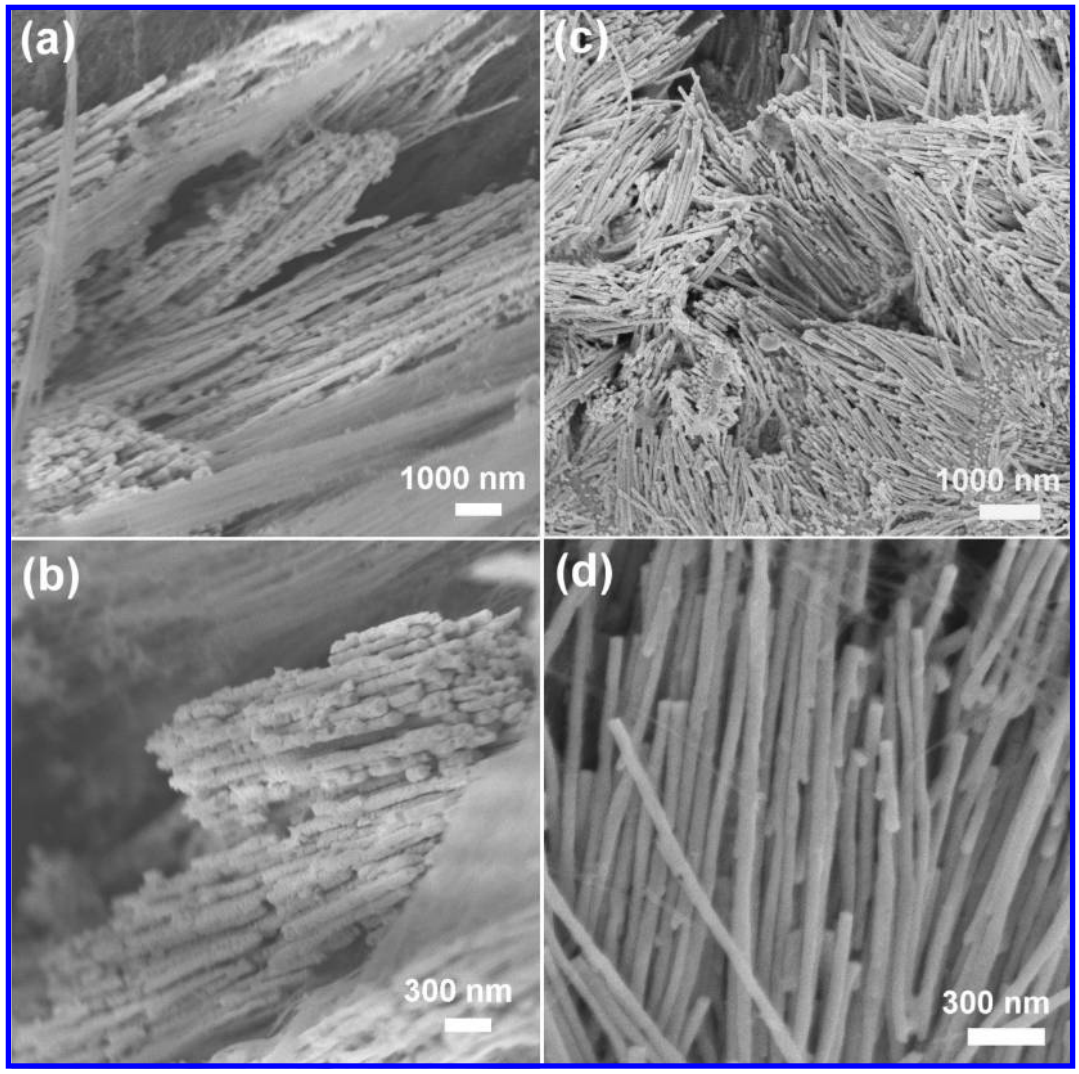

Figure 3. (a) FE-SEM image of as-prepared $CoPt_3$ nanowires. (b) Magnified FE-SEM image of as-prepared $CoPt_3$ nanowires. (c) FE-SEM images of $CoPt_3$ nanowires after thermal treatment (700 °C, 5 h). (d) Magnified FE-SEM image of $CoPt_3$ nanowires after thermal treatment (700 °C, 5 h).

state, the rearrangement of atoms depends not only on energy but also on their mobility in the lattice. Structural defects favor the mobility of atoms in the lattice, as found in an earlier study that involved the synthesis of Ag-doped FePt nanoparticles,[3c] in which Ag segregation during annealing generated structural vacancies and increased the mobility of the Fe and Pt atoms, reducing the annealing temperature.

Magnetic Analysis. Figure 4 plots the hysteresis loops of the $CoPt_3$ nanowires with/without annealing in external fields perpendicular (⊥) and parallel (//) to the nanowires at room temperature. Typical magnetic anisotropy behavior is observed for the $CoPt_3$ nanowire arrays; the coercivity and squareness were higher when the field was applied parallel to the axis of the nanowires than when the field was perpendicular to it. To reduce the magnetostatic energy, the magnetostatic vector lies preferentially along the wire axis. Thus, the direction of magnetization of the nanoarrays is along the axis of the nanowires. Figure 4b plots the variation in the coercivity and squareness with the annealing temperature of the $CoPt_3$ nanowires when the external field is applied perpendicular to the long axes of the nanowires. Notably, *Hc* rapidly increases upon annealing at 700 °C (∼1422 Oe). It is well-known that the crystallographic structure, chemical composition, diameter, and aspect ratio of the wires affect the magnetic properties.[11b] Reducing the diameter of nanowires improves the hardness of the magnetic hysteresis and raises the coercivity. This is owing to a reduction in macroscopic interactions between nanomagnets and enhancement of the switching field of the individual nanowires. The crystallographic structure and chemical composition were essential to controlling the magnetic character herein because of the presence of nonmagnetic properties of the Pt phase formed in the deposited nanowires. In the low temperature condition (below 600 °C), the cobalt phase contributes greatly to the magnetic character in terms of *Hc*. The partial alloying of Co and Pt atoms upon thermal treatment (700 °C) dominates the magnetic performance. Figure 4c plots a typical $M-H$ loop for $CoPt_3$ nanowires that are annealed at various temperatures in an anodic alumina template, measured in a magnetic field that is parallel to the nanowires. The coercivity and squareness of the $CoPt_3$ nanowires that were annealed at 700 °C were ∼1806 Oe and ∼0.7, respectively. Interestingly, the magnetic properties of the $CoPt_3$ nanowires are enhanced. Figure 4d plots the variation in parallel coercivity and squareness of the $CoPt_3$ nanowires with annealing temperature. When the annealing temperature was increased from 500 to 600 °C, the coercivity changed slightly. It could be found

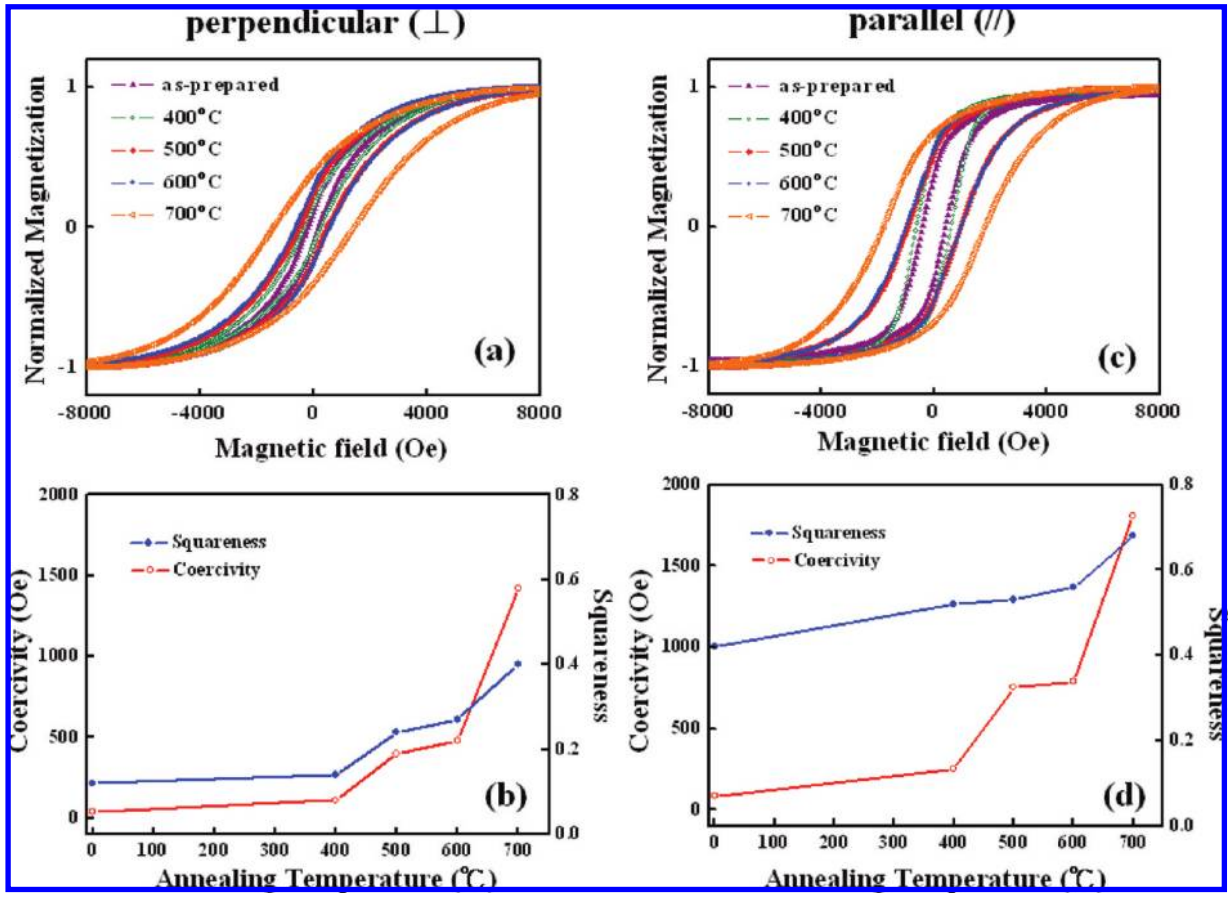

Figure 4. (a) Typical hysteresis loop of $CoPt_3$ nanowire arrays annealed at desired temperature, measured in a field applied perpendicular to the wires. (b) Variation of perpendicular coercivity and squareness with annealing temperature for $CoPt_3$ nanowires. (c) Typical hysteresis loop of array of $CoPt_3$ nanowires annealed at desired temperature, obtained in applied field parallel to wires. (d) Variation of parallel coercivity and squareness with annealing temperature for $CoPt_3$ nanowires.

that the parallel coercivity increases drastically with annealing temperature up to 700 °C, reaching a maximum of ∼1800 Oe, which exceeds that of $CoPt_3$ nanowires in a perpendicular field. The effect of annealing temperature on the squareness is similar to that of coercivity.

Structural Analysis via XAS. To verify further the local structure of the synthesized bimetallic nanowires, XAS analyses were performed. Since XAS is sensitive to atomic local sites and does not depend on the long-range order of the atomic arrangement, it is a powerful approach for analyzing the local structure of these multicomponent nanomaterials. The local structures are examined by comparing the Co K-edge and Pt L_{III}-edge X-ray absorption spectra with those of the corresponding metal foil. Figure 5a presents normalized X-ray absorption near edge structure (XANES) spectra of $CoPt_3$ nanowires for various annealing temperatures. Broad white line peaks of nanowires after annealing above 600 °C are separated into distinct peaks, B (as indicated by arrows in Figure 5a), which are characteristic of alloyed CoPt.[17] The A and B features are assigned to transitions from 1s to the unoccupied final states that originate from hybridized 4s, 4p, and 3d levels. These final states are generally described as having mainly 3d character for feature (A) and s−p character for feature (B). These two

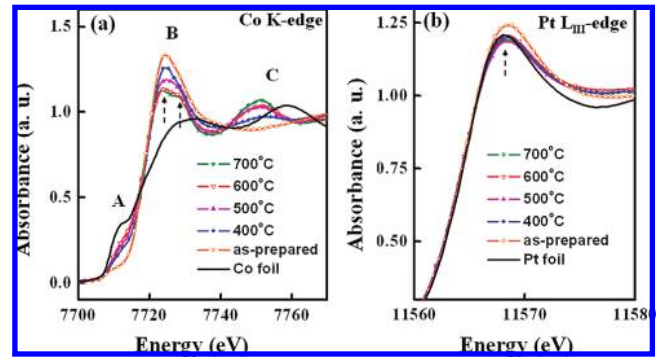

Figure 5. Co K-edge XANES (a) and Pt L_{III}-edge XANES (b) spectra upon thermal annealing of $CoPt_3$ nanowires at desired temperature.

features vary strongly upon alloying of Co and Pt, reflecting a population rearrangement between the levels associated with these two transitions. Increasing the annealing temperature under reducing conditions can deliver sufficient energy to reduce the cobalt ion and increase the proportion of zerovalent cobalt in the $CoPt_3$ nanowire. However, the absorption peak (feature A) of the sample that was treated at 700 °C is higher than that of the Co foil, revealing the presence of the oxidation states of cobalt in the $CoPt_3$ nanowires, but in a lower amount than in the other samples. For the Pt L_{III}-edge XANES spectra, the decline in the intensity of the white line peak caused charge transfer from Co to Pt, suggesting the progress of Co−Pt

(17) (a) Park, J.-I.; Kim, M. G.; Jun, Y.-W.; Lee, J. S.; Lee, W.-R.; Cheon, J. *J. Am. Chem. Soc.* **2004**, *126*, 9072. (b) Hill, E. K.; Baudoing-Sanois, R.; Moraweck, B.; Renouprez, A. J. *J. Phys. Chem.* **1996**, *100*, 3102.

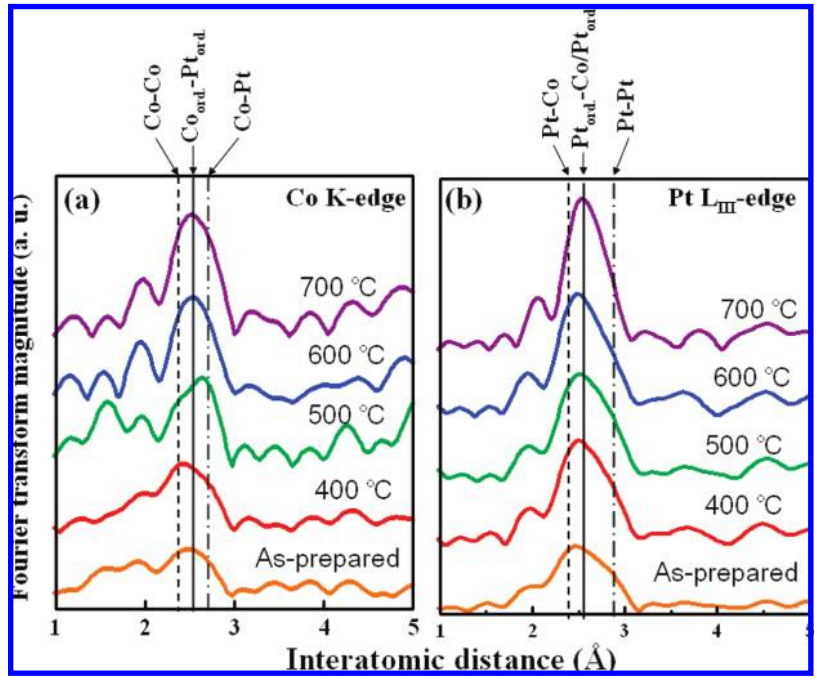

Figure 6. EXAFS spectra of Co K-edge (a) and Pt L_{III}-edge XANES (b) upon thermal annealing of $CoPt_3$ nanowires at desired temperature, and of corresponding foil.

alloying associated with the annealing effect.[17a,18] More precisely, the white line in the L_{III}-edge involved the two allowed transitions $2p_{3/2} \rightarrow 5d_{5/2}$ and $2p_{3/2} \rightarrow 5d_{3/2}$ bands. The general decrease in the white line intensity, as Pt is progressively mixed with Co, points to progressive filling of the 5d band. This phenomenon is generally associated with the alloying of the Pt-3d transition metal.[17b]

The physical properties of nanomaterials can be determined by their structural phase transitions: this phenomenon is essential to any significant improvement of their magnetic properties. EXAFS was conducted to obtain better evidence of the structural parameters of Co/Pt bimetallic nanowires. Figure 6 shows the Co K-edge and Pt L_{III}-edge of $CoPt_3$ nanowires that had been annealed at the desired annealing temperature. A broad peak at ~2.5 Å was observed in the Fourier transform (FT) of the Co K-edge EXAFS spectra of the as-prepared $CoPt_3$ nanowires before phase correction, suggesting that central Co atoms were randomly surrounded by Co and Pt atoms. In the EXAFS spectrum of $CoPt_3$ nanowires that had been annealed at 400 °C, a strong peak at ~2.4 Å and a shoulder at ~2.6 Å obtained before phase correction indicate that the first shell around the Co atoms included neighboring atoms of two elements. The peak at ~2.4 Å is assigned to single scattering by Co−Co atoms, and the shoulder at ~2.6 Å corresponds to single scattering by the Co−Pt atoms. The intensity of the FT peak at ~2.6 Å increased and was higher than that of Co−Co scattering, as the annealing temperature approached 500 °C, revealing that the first shell around the Co atoms was a shell of Pt atoms rather than Co atoms. Since the Co/Pt ratio was close to 1/3, the scattering of the Pt atoms was amplified. In a bimetallic system, a homobond pair is preferentially formed, and so the associated structure it called a "homobond-philic" structure.[19] It is also called a cluster-in-cluster structure, in which like atoms together

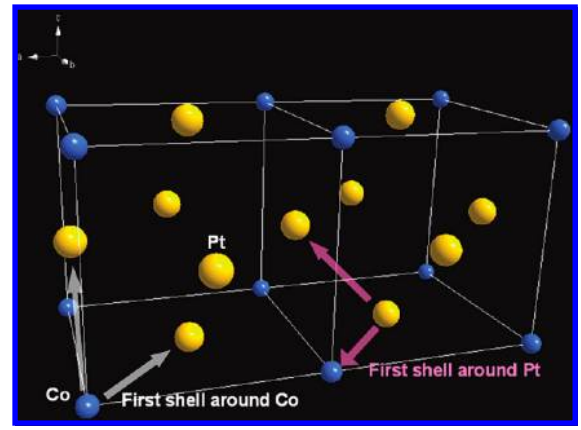

Figure 7. Face-centered cubic structure of $CoPt_3$ and first shell scattering modes of Co/Pt atoms.

form small clusters, which randomly mix to form larger clusters. In the early stage (annealing in 400 °C), the homobond-philic structure was initially present, and the formation of a homobond (Co−Co) rather than a heterobond (Co−Pt) was observed. As the temperature further increased, enough energy was provided to the Co/Pt atoms to cause them to interdiffuse, increasing the intensity of scattering from the Pt atoms. Upon annealing above 600 °C, the FT peaks that corresponded to single scattering by Co−Co and Co−Pt atoms disappeared and another peak appeared at ~2.5 Å; this could be attributed to the existence of only Pt atoms in the first scattering shell around the Co atoms in the ordered structure ($L1_2$) (Figure 7). This observation implies structural evolution from fcc to ordered $L1_2$ which was consistent with the result of XRD. With regard to Pt atoms, the EXAFS spectrum of as-prepared $CoPt_3$ nanowires before phase correction included a strong peak at ~2.4 Å and a shoulder at

(18) Ely, T. O.; Pan, C.; Amiens, C.; Chaudret, B.; Dassenoy, F.; Lecante, P.; Casanove, M.-J.; Mosset, A.; Respaud, M.; Broto, J.-M. *J. Phys. Chem. B* **2000**, *104*, 695.

(19) Bian, C.-R.; Suzuki, S.; Asakura, K.; Ping, L.; Toshima, N. *J. Phys. Chem. B* **2002**, *106*, 8587.

Table 1. Co K-Edge EXAFS Structural Parameters of $CoPt_3$ Nanowires with/without Thermal Treatment

sample	path	R (Å)	CN	σ^2 (Å^2)	ΔE (eV)
as-prepared	Co−Co	2.46(6)	1.9(4)	0.0101(6)	3.7(6)
	Co−Pt	2.63(7)	5.9(7)	0.009(2)	−2.4(5)
400 °C	Co−Co	2.43(5)	3.9(9)	0.0091(5)	3.1(5)
	Co−Pt	2.65(5)	5.6(8)	0.009(7)	−2.8(7)
500 °C	Co−Co	2.41(4)	2.1(4)	0.0086(6)	4.2(6)
	Co−Pt	2.66(2)	7.5(8)	0.0089(2)	1.1(3)
600 °C	Co−Pt($L1_2$)	2.72(3)	9.8(6)	0.0088(3)	5.2(7)
700 °C	Co−Pt($L1_2$)	2.73(3)	10.8(4)	0.0074(2)	4.8(6)

Table 2. Pt L_{III}-Edge EXAFS Structural Parameters of $CoPt_3$ Nanowires with/without Thermal Treatment

sample	path	R (Å)	CN	σ^2 (Å^2)	ΔE (eV)
as-prepared	Pt−Co	2.64(2)	1.9(5)	0.0073(4)	7.3(5)
	Pt−Pt	2.73(6)	6.2(9)	0.0086(5)	1.2(3)
400 °C	Pt−Co	2.66(4)	2.0(4)	0.0078(3)	−5.2(5)
	Pt−Pt	2.72(3)	8.4(8)	0.0071(5)	−2.2(4)
500 °C	Pt−Co	2.63(4)	2.5(7)	0.0089(5)	3.5(3)
	Pt−Pt	2.73(6)	8.0(3)	0.0064(3)	−4.2(5)
600 °C	Pt−Co($L1_2$)	2.71(9)	2.8(5)	0.0073(3)	5.8(7)
	Pt−Pt	2.73(4)	7.2(6)	0.0060(5)	3.2(4)
700 °C	Pt−Co($L1_2$)	2.72(6)	3.2(3)	0.0055(6)	3.9(7)
	Pt−Pt($L1_2$)	2.73(3)	7.4(7)	0.0066(8)	−1.5(4)

∼2.8 Å, indicating that the first shell around the Pt atoms included neighboring atoms of two elements. The peak at ∼2.4 Å is assigned to single scattering by Pt−Co atoms, and the shoulder at ∼2.8 Å corresponds to single scattering by the Pt−Pt atoms. When the nanowires were thermally annealed, Co and Pt atoms migrated significantly. As the migration of Co and Pt atoms progressed, the FT peaks that corresponded to single scattering of Co−Co and Co−Pt atoms disappeared. Consequently, another peak that appeared at ∼2.6 Å after thermal treatment may be attributable to Co and Pt atoms being in identical positions in the first scattering shell around the Pt atoms in the ordered structure ($L1_2$) (Figure 7). This result is characteristic of the structural transition of the Co−Pt bimetallic system. Structural parameters from each spectrum are obtained by EXAFS refinement (Tables 1 and 2). The EXAFS spectra of Co K-edge and Pt L_{III}-edge were adopted to determine the structural parameters based on a two-shell model that involves Co−Co, Co−Pt, Pt−Co, and Pt−Pt shells to characterize the short-range structure around Co and Pt atoms. In the case of as-prepared $CoPt_3$ nanowires, these results suggest that the interatomic distance between Co and the nearest neighboring Co atoms is 2.46 Å, which is consistent with the value for the bulk face-centered cubic (fcc) phase of cobalt (2.50 Å). Additionally, the interatomic distance between Pt and the nearest neighboring Pt atoms is determined to be 2.73 Å, which agrees closely with that reported for Pt nanoparticles (2.75 Å). The interatomic distance between Co and Pt atoms did not change significantly as the annealing temperature increased (400 and 500 °C), suggesting that neither structural contraction nor expansion occurred in this stage. Nevertheless, the first-metal distance, which was increased to ∼2.7 Å in the samples that were annealed above 600 °C, is a Co−Pt bond length that is similar to that expected (2.72 Å) in the ordered structure ($L1_2$). The structural parameters of Pt−Co and Pt−Pt in the first shell are obtained as 2.72 and 2.73 Å, which are also consistent with 2.72 Å in the $CoPt_3$ $L1_2$ model. Both of these observations further verify the occurrence of a structural phase transition and the formation of an $L1_2$ ordered phase.

The coordination number (CN) was also utilized to characterize the phase transition in the nanowires. The result of refinement was characteristic of the bimetallic nanomaterials. A simple relationship is satisfied when both Co and Pt atoms are randomly distributed in the nanowires (random alloy).[20]

$$N^{\mathrm{CoPt}} = (X_{\mathrm{Pt}}/X_{\mathrm{Co}})N^{\mathrm{PtCo}}$$

N^{CoPt} is the coordination number of the Pt atoms around the Co atoms, and N^{PtCo} is the coordination number of the Co atoms around the Pt atoms. X_{Pt} and X_{Co} denote the atomic fractions of Pt and Co in the sample, respectively. Notably, the coordination number determined from the EXAFS spectra of the as-prepared $CoPt_3$ nanowires satisfies the aforementioned relationship, indicating that $CoPt_3$ nanowires before annealing had random alloy structures. As the temperature was increased, the coordination number changed significantly. When the annealing temperature reached 400 or 500 °C, the CN of Co/Pt around the Co and Pt atoms did not satisfy the above relationship. The CNs of both the Co−Co and the Pt−Pt paths significantly exceeded that derived from the above relationship, revealing that Co and Pt atoms exhibited "cluster-in-cluster" structure upon annealing at 400 or 500 °C. When the temperature exceeded 600 °C, the Co K-edge results revealed only the Co−Pt ($L1_2$) path. As the temperature increased, the coordination number of the Co−Pt path increased from 9.8 (600 °C) to 10.8 (700 °C). From the results for the Pt L_{III}-edge, the scattering atoms around Pt atoms were both Co and Pt atoms. Most interestingly, the Co and Pt atoms are located in an equal distance around Pt atoms, since Co and Pt atoms have similar scattering distances (as displayed in Figure 7). As a result, the above observation confirmed the phase transition and formation of a chemically ordered phase ($L1_2$), the local structure of the nanowires transitioned from disordered fcc to cluster-in-cluster, and $L1_2$.

Mechanism. Based on the above observations, we propose a model of the growth mechanism of $CoPt_3$ nanowires that includes a phase transition (as depicted in Scheme 1). $CoPt_3$ nanowires were codeposited on an amorphous gold film on the back of AAO. In the initial stage of $CoPt_3$ growth, the orientation of the nuclei was random and a newly coalesced compact deposit exhibited a perfectly random orientation. The rapid growth of low-surface-energy grains at the expense of high-energy grains resulted in an increase in grain size, favoring the formation of columnar grains. Following, the confinement of a porous nanostructure in the AAO templates facilitated the formation of the nanowires. As-prepared $CoPt_3$ nanowires with a lower degree of crystallinity exhibited density defects and intrinsic stress because of the codeposition of Co and Pt. The anisotropy that was induced by stress may have directly competed with the shape anisotropy, reducing the coercivity and squareness.[11f] Hence, the magnetic domains (as indicated by arrows) randomly orientated and were small. Thermal treatment increased the coercivity and squareness by structural relaxation and reducing the number of defects. Furthermore, the magnetostatic vector is well-known to lie preferentially along the wire axis to reduce the magnetostatic energy. Accordingly, the direction of magnetization of the nanoarrays was along the axis of the nanowires, causing the *Hc* of the parallel field to exceed that of the perpendicular field. After annealing at 400 °C, $CoPt_3$ nanowires have a "cluster-in-cluster structure", their magnetic nature bring

(20) (a) Chen, H. M.; Liu, R. S.; Asakura, K.; Lee, J.-F.; Jang, L.-Y.; Hu, S. F. *J. Phys. Chem. B* **2006**, *110*, 19162. (b) Toshima, N.; Harada, M.; Yamazaki, Y.; Asakura, K. *J. Phys. Chem.* **1992**, *96*, 9927.

Scheme 1. Phase Transition Mechanism: Local Structure, Atomic Distribution, and Corresponding Magnetic Domain[a]

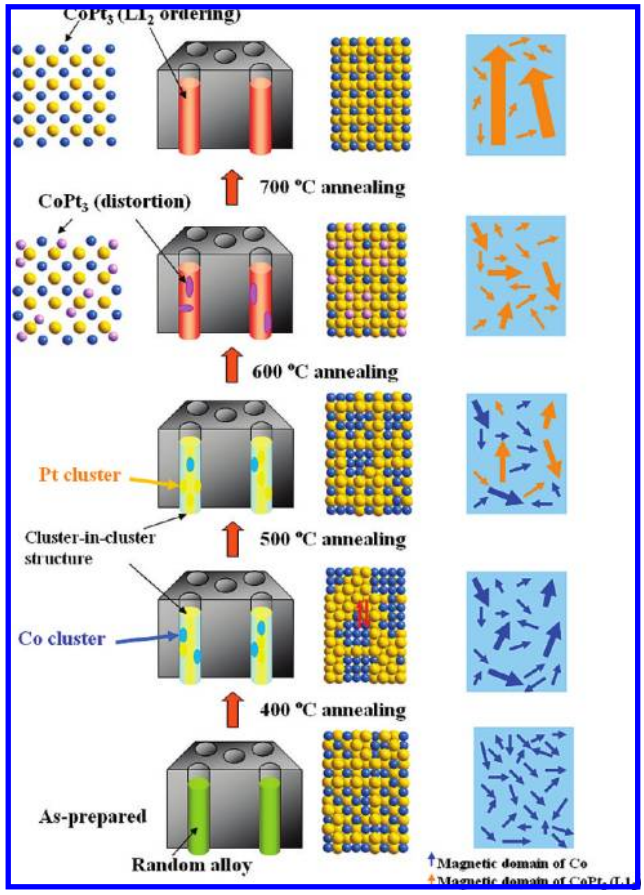

[a] Co and Pt atoms are depicted as blue and yellow balls, respectively. Arrows indicate individual magnetic domains.

attributable to the ferromagnetic cobalt nanoclusters at this stage. The platinum played a particular role in determining the magnetic behavior. Platinum atoms isolated each Co cluster and facilitated the formation of Co nanoclusters with a single magnetic domain. This effect was similar to that observed in bamboo-like multilayered nanowires.[21] As the annealing temperature was further increased (500 °C), as a matter of fact, a significant effect was occurring although the $CoPt_3$ nanowires retained their cluster-in-cluster structure. Co and Pt atoms began to migrate by "interdiffusion", forming a chemically ordered structure ($L1_2$), causing a strong ferromagnetic coupling between Co and Pt atoms owing to the hybridization of Co 3d and Pt 5d orbitals and the spin polarization of Pt atoms.[17a,18] Both the Co cluster (blue arrows in Scheme 1) and the $CoPt_3$ ordered structure (yellow arrows in Scheme 1) contributed to the magnetic properties of the nanowires (3-fold increase in *Hc*). Following annealing at over 600 °C, many defects were present in the nanostructure, despite the phase transformation most Co−Pt atoms (as revealed by EXAFS), which suppressed the enhancement of coercivity and squareness. Although the formation of an $L1_2$ phase could increase the magnetic performance in terms of coercivity and squareness, it destroyed the Co−Co coupling simultaneously and reduced the contribution of the Co clusters to the magnetic character. As shown in Scheme 1, only $CoPt_3$, indicated by yellow arrows, was present in the magnetic domain. Consequently, the coercivity and squareness were lightly higher than those following annealing at 500 °C. Finally, most of the $CoPt_3$ nanowires had a long-range ordered structure following annealing above 700 °C, and the coercivity and squareness were significantly increased by the reduction in the number of defects and the number of $CoPt_3$ grains that grew.

Conclusion

The nanoscale characterization of $CoPt_3$ nanowires and the correlation of nanostructures with magnetic properties during phase transition were successfully demonstrated. EXAFS data clearly verify that $CoPt_3$ nanowires undergo a phase transition. The occurrence of subsequent thermally induced phase transitions in the $CoPt_3$ nanowires was clearly confirmed. A thermally induced phase transition of $CoPt_3$ nanowires to ordered $L1_2$ $CoPt_3$ through a "cluster-in-cluster" intermediate state *via* interdiffusion was identified. XAS results were used to elucidate a proper scheme for the phase transition process. Although this study concerned the Co and Pt system, we believe that this strategy can also be extended to other bimetallic systems.

Acknowledgment. The authors would like thank the National Science Council of the Republic of China, Taiwan (Contract Nos. NSC 97-2113-M-012-MY3 and NSC 97-2112-M-003-007-MY3) and the Ministry of Economic Affairs of the Republic of China (Contract Nos. 97-EC-17-A-08-S1-006 and 97-EC-17-A-01-S1-026) for financially supporting this research.

Supporting Information Available: Elemental analysis of CoPt nanowires was conducted using an EDS (S1). This material is available free of charge via the Internet at http://pubs.acs.org.

JA906103P

(21) (a) Lee, J. H.; Wu, J. H.; Liu, H. L.; Cho, J. U.; Cho, M. K.; An, B. H.; Min, J. H.; Noh, S. J.; Kim, Y. K. *Angew. Chem., Int. Ed.* **2007**, *46*, 3663. (b) Skinner, K.; Dwyer, C.; Washburn, S. *Nano Lett.* **2006**, *6*, 2758.